Granular fountains: Convection cascade in a compartmentalized granular gas

Devaraj van der Meer,[1] Ko van der Weele,[1,2] and Peter Reimann[3]
[1]*Department of Science and J. M. Burgers Centre for Fluid Dynamics, University of Twente, P. O. Box 217, 7500 AE Enschede, The Netherlands*
[2]*Mathematics Department, University of Patras, 26500 Patras, Greece*
[3]*Department of Physics, University of Bielefeld, 33615 Bielefeld, Germany*
(Received 30 January 2006; published 22 June 2006)

This paper extends the two-compartment granular fountain [D. van der Meer, P. Reimann, K. van der Weele, and D. Lohse, Phys. Rev. Lett. **92**, 184301 (2004)] to an arbitrary number of compartments: The tendency of a granular gas to form clusters is exploited to generate spontaneous convective currents, with particles going down in the well-filled compartments and going up in the diluted ones. We focus upon the bifurcation diagram of the general K-compartment system, which is constructed using a dynamical flux model and which proves to agree quantitatively with results from molecular dynamics simulations.

DOI: 10.1103/PhysRevE.73.061304 PACS number(s): 45.70.−n, 02.30.Oz, 05.60.Cd

I. INTRODUCTION

The most prominent feature of a granular gas is the fact that energy is dissipated in every collision of the particles. In order to keep the particles in a gaseous state, a continuous supply of energy is needed, so granular gases are intrinsically far from thermodynamic equilibrium; this results in many remarkable properties unseen in any ordinary molecular gas [1,2]. One striking example of such a property is the tendency to spontaneously separate into dense and dilute regions, known as *clustering* [3–5], which can be demonstrated in a particularly clear-cut form in a vertically vibrated container that is divided into K connected compartments [6–8].

In many experimental situations, the energy the system needs is supplied from one of the boundaries, i.e., the gas is vibrated ("heated") from one of the sides [9]. In ordinary fluids this type of heating is known to produce convective currents, and similar currents have also been reported in granular systems, where they go hand in hand with the clustering effect [10–12]: Patterns of dense (cold) regions streaming towards the wall alternated with dilute (hot) streams directed from the walls into the system. Here "cold" and "hot" refer to the granular temperature, which is proportional to the average squared velocity fluctuations of the particles around the mean flow.

In this paper we exploit this connection between convection and clustering: The original K-compartment system used to demonstrate clustering is modified in such a way that it spontaneously generates convective currents. Whereas in the original system the compartments were connected only via a slit at a certain height h in the separating wall [6,8], we now add a small hole at the bottom ($h=0$). In a recent Letter [13] we introduced the two-compartment version of this modified system, and discussed the transition from the uniform state (with both compartments equally filled) to the clustered state shown in Fig. 1(a). The latter state exhibits a convective flow of particles, reminiscent of how water moves through a fountain, and that is why we called it a *granular fountain*.

Here we will go beyond the two-compartment system and study an arbitrary number of compartments, both theoretically and numerically, revealing the increasingly intricate structure of the transition for growing K, which involves a whole cascade of convective states.

In Sec. II we describe, after a brief review of the case $K=2$, the results of molecular dynamics simulations in cyclic systems of $K=3$ and $K=5$ compartments. These show that for decreasing shaking strength there is a stepwise transition from the uniform state with K hot compartments, to a one-cluster state [one cold compartment and $K-1$ hot ones; see Fig. 1(d)], to a two-cluster state [two cold compartments and $K-2$ hot ones; see Fig. 1(c)], and so on, until at some low shaking strength one arrives at a situation with K cold compartments, which is again a uniform state. This transition is found to be strongly hysteretic, with the successive steps in the opposite direction (i.e., for *increasing* shaking strength) taking place at different values of the shaking strength. To quantitatively explain these observations we use the flux model introduced in [13], which we describe in Sec. III. The technique to find the associated bifurcation diagram (showing the complete cascade) is described in Sec. IV, and we explicitly work out the cases $K=3$ and 5, finding good agreement with the numerical diagrams found earlier. In Sec. V we make concluding remarks. The paper is accompanied by a mathematical Appendix, where we rule out the existence of fountain states in which the particle content of the compartments in the long-time limit would vary periodically or chaotically.

II. NUMERICAL EXPERIMENTS

Here we describe our observations in molecular dynamics simulations of the granular fountain in a phenomenological way. After a brief review of experiments and simulations of the two-compartment fountain, we proceed to the description of the results of molecular dynamics simulations in systems consisting of $K=3$ and $K=5$ compartments.

A. Review of $K=2$ compartments

Before we come to the numerical simulations for $K\geq 3$ compartments, it is useful to first recapitulate the case of two compartments [13].

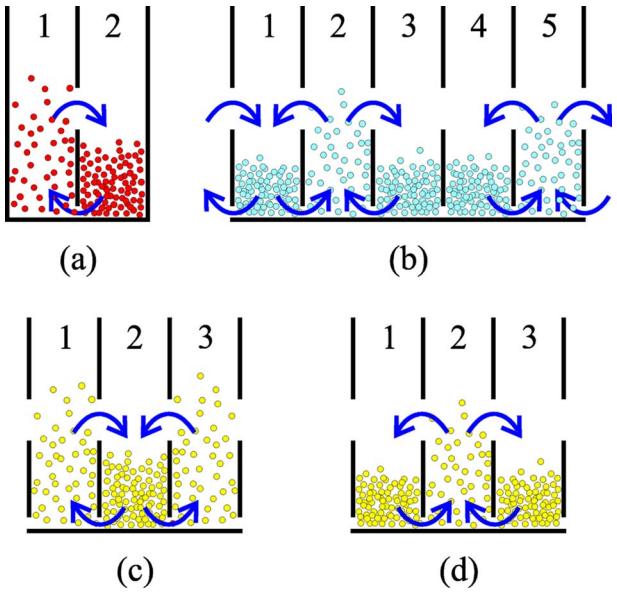

FIG. 1. (Color online) (a) Granular fountain in $K=2$ compartments: the clustering effect induces a steady convective current in the system [13]. (b) One of the convection patterns for a cyclic array of $K=5$ compartments. (c), (d) The two convective states in a cyclic array of $K=3$ compartments. Both states are threefold degenerate, since the cluster (the region of low density) can be located in any of the three compartments.

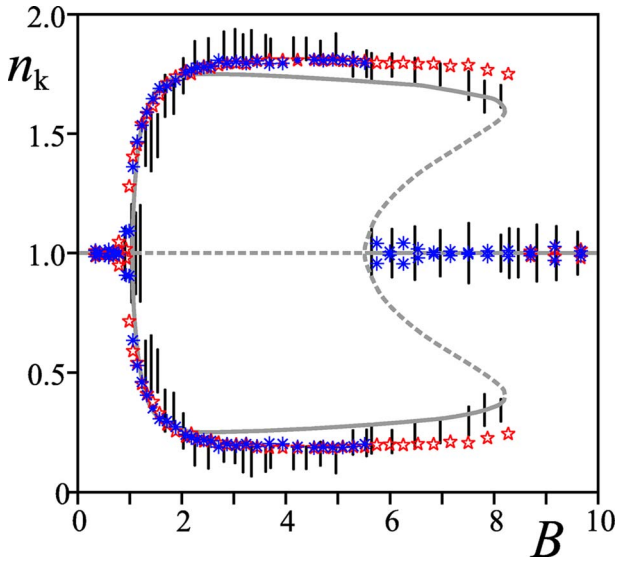

FIG. 2. (Color online) Bifurcation diagram for the two-compartment granular fountain, depicting the steady states of the system as a function of the driving parameter B defined in Eq. (2) (from [13]). This diagram contains experimental measurements [indicated by the (black) error bars], data from molecular dynamics simulations using uniform (asterisks) and clustered (stars) initial conditions, and the theoretical prediction from our flux model described in Sec. III (gray lines) with $\lambda=0.018$. The stable states are indicated by a solid line, the unstable ones by a dashed line. The model parameter λ, representing the ratio of the fluxes through hole and slit in the limit of very strong shaking, will be defined more precisely in Sec. III.

When the system is shaken sufficiently strong, or equivalently, when the driving parameter $B \propto (af)^{-2}$ is sufficiently small [with a and f the amplitude and frequency of the driving; see Eq. (2) for the precise definition of B], the particles do not cluster and hence no convection occurs. When the value of B exceeds a certain critical threshold, however, the particles spontaneously cluster into one of the compartments [see Fig. 1(a)] and this creates an imbalance around the hole at the bottom. The greater pressure from the dense compartment causes a net flow of particles through the hole into the dilute compartment; and the particles that enter the dilute compartment soon gain enough kinetic energy from the vibrating bottom to jump through the slit again. A steady state sets in, in which the flow through the hole is balanced by an equally strong flow (in the opposite direction) through the slit. In this way the clustering effect in a compartmentalized granular gas leads to a steady convective flow.

For the two-compartment system we found that the transition from the uniform state to the fountain state (upon increasing the value of B) occurs through a pitchfork bifurcation, i.e., a continuous second-order phase transition. This is shown in the bifurcation diagram of Fig. 2. When B is increased even further, the fountain state breaks down and gives way to the uniform state again, this time via a discontinuous, first-order phase transition [13]. In this high-B regime, the shaking is so weak that the particles do not get sufficient kinetic energy anymore to jump through the slit (not even in a diluted compartment) and the only effective opening is the hole at the bottom, via which a uniform equilibrium is established.

B. $K=3$ compartments

The above general scenario (uniform hot state → clustered fountain state → uniform cold state) still holds if we add more compartments to the system, but now the system goes through more than just one intermediate fountain state. For example, for $K=3$ there are *two* fountain states: one with one cluster [Fig. 1(c)] and one with two clusters [Fig. 1(d)]. Another difference from the case of two compartments is that the one-cluster state is created from the hot uniform state *not* via a continuous (second-order) phase transition, but via a discontinuous (first-order) one, involving hysteresis. This means that all transitions in the three-compartment system are hysteretic, and in fact we find that the two fountain states and the uniform state coexist for a considerable interval of B values. Therefore, to find which states are stable at a given value of B we have to explore all possible steady states as initial conditions.

We performed event-driven molecular dynamics simulations of a system of $K=3$ compartments, arranged cyclically (periodic boundary conditions) and connected by slits of 5.00×50.0 mm^2 (starting at a height $h=25.0$ mm above the bottom) and holes of 4.20×4.20 mm^2 (starting immediately at the bottom) located in the center of the separating walls. Each compartment has a ground area of $\Omega=19.4\times50.0$ mm^2 and contains, in the uniform situation, 200 particles with a radius of $r=1.18$ mm and a normal restitution coefficient of $e=0.90$. Thus the total number

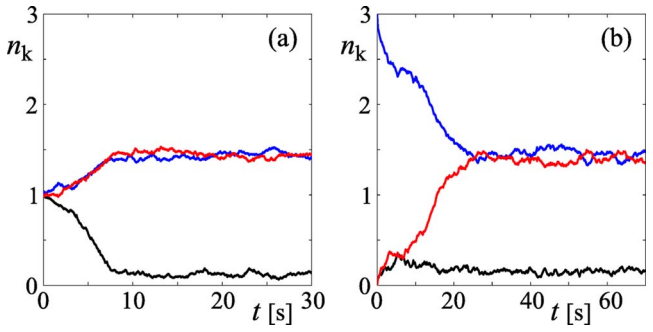

FIG. 3. (Color online) Two typical time-evolution plots of the cyclic three-compartment granular fountain, obtained from particle simulations with 600 particles. The quantity n_k along the vertical axis denotes the particle fraction in compartment k with respect to the uniform distribution: $n_k=N_k/200$, with N_k the number of particles in compartment k. (a) starting from the uniform distribution, with 200 particles in each compartment, at $(af)^{-2}=1.11\times10^3$ $(\mathrm{m/s})^{-2}$; (b) starting from the clustered state in which one compartment contains all 600 particles, at $(af)^{-2}=1.89\times10^3$ $(\mathrm{m/s})^{-2}$. In both cases the system evolves to a steady two-cluster state in which two compartments share most of the particles and one compartment is nearly empty.

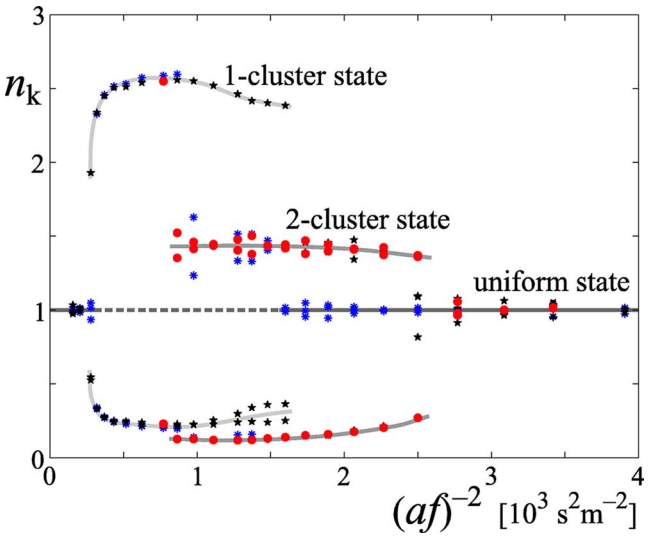

FIG. 4. (Color online) Bifurcation diagram of the cyclic granular fountain with $K=3$ compartments, from particle simulations with 600 particles. Asterisks (blue) are steady states obtained from the uniform initial distribution with 200 particles in each compartment; stars (black) are reached from an initial one-cluster state; solid dots (red) are obtained from an initial two-cluster state. The gray curves (drawn as aids to the eye) outline the stable branches of the bifurcation diagram (cf. Fig. 9); the dashed line represents the interval where the uniform state is unstable.

of particles in the three-compartment system is $N_{tot}=600$. The system is driven vertically with a triangular signal of which the strength $[\propto(af)^2]$ is varied by changing the frequency f whereas the amplitude is kept at a constant value of $a=1.00$ mm (i.e., a peak to peak amplitude of 2.00 mm).

Figure 3 shows two typical time-evolution plots for this system. The left plot, at an inverse driving strength of $(af)^{-2}=1.11\times10^3$ $(\mathrm{m/s})^{-2}$, starts from an unstable uniform distribution of 200 particles in each compartment (i.e., the particle fraction n_k in each compartment with respect to the uniform distribution is equal to 1) and ends up in a two-cluster state [depicted in Fig. 1(d)] for which $n_k\approx1.45$ in two of the compartments, and ≈0.10 in the third compartment. For a somewhat weaker driving strength of $(af)^{-2}=1.89\times10^3$ $(\mathrm{m/s})^{-2}$ there still exists a steady two-cluster state, but it is not reachable anymore from the uniform distribution since this has become stable itself. Instead, it can now be reached from the unstable one-cluster state, as shown in Fig. 3(b).

A series of simulation runs like the ones just described, at different values of the shaking strength and from a variety of initial states, yields the bifurcation diagram of Fig. 4. It contains all attainable steady states of the three-compartment system as a function of the inverse driving strength $(af)^{-2}$ $(\propto B)$: Starting at strong driving (left in the diagram) we first see the uniform state, which is stable up to $(af)^{-2}=0.56\times10^3$ $(\mathrm{m/s})^{-2}$. When it becomes unstable, the system goes over to the stable one-cluster state depicted in Fig. 1(c). Lowering the shaking strength even more, a second stable state comes into existence characterized by two dense compartments and one dilute [see Fig. 1(d)]. These two convective states coexist for a certain interval of the shaking strength until the one-cluster state ceases to be stable; at approximately the same value of $(af)^{-2}$ the uniform state regains its stability. For even lower shaking strength the two-cluster state becomes unstable too [around $(af)^{-2}=2.70\times10^3$ $(\mathrm{m/s})^{-2}$], leaving the uniform distribution the only stable state in the system.

C. $K=5$ compartments

The bifurcation diagram for a cyclic array of five compartments, Fig. 5, follows the same pattern, this time with a true cascade of fountain states (with a successively growing number of clusters) acquiring and losing stability. Upon decreasing the shaking strength we find, just as for $K=3$, that the uniform distribution loses stability in what appears to be a first-order phase transition (this will be confirmed later in Fig. 11): the system jumps immediately to a well-developed one-cluster state at $(af)^{-2}=0.20\times10^3$ $(\mathrm{m/s})^{-2}$. Lowering the shaking strength we find two-, three-, and four-clustered fountain states gaining stability one after the other; as an example we have depicted a three-cluster state in Fig. 1(b). Note that at $(af)^{-2}\approx1.35\times10^3$ $(\mathrm{m/s})^{-2}$ the two-, three-, and four-clustered states are simultaneously stable, illustrating once more that one really has to explore a variety of initial states to find all possible end states. Two small clouds of data points, all originating from an initial one-cluster state, have been shaded in Fig. 5: Here the system got stuck in either its initial state (upper cloud) or in a three-cluster state (lower cloud). We come back to this in Sec. IV C, where we will see that at low shaking strengths the transition from one configuration to the other may easily be hindered by these side effects.

At some low shaking strength [around $(af)^{-2}=1.80\times10^3$ $(\mathrm{m/s})^{-2}$] the uniform distribution regains stability, and

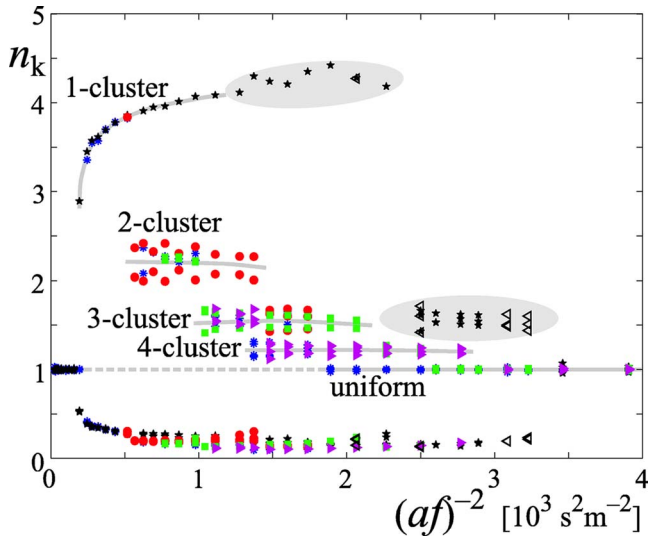

FIG. 5. (Color online) Bifurcation diagram, obtained from particle simulations with 1000 particles, showing the stable steady states of the cyclic five-compartment system. The various symbols denote the different initial states of the simulation: asterisks (blue) are obtained from a uniform initial distribution (200 particles in each compartment); stars (black) and open triangles (black) from a one-cluster state; solid dots (red) from a two-cluster state; squares (green) from a three-cluster state; triangles (magenta) from an initial four-cluster state. The gray lines help to distinguish the stable branches of the bifurcation diagram (cf. Fig. 11). Unlike in Fig. 4, here the fractions in the dilute compartments belonging to each of the multicluster states cannot be distinguished from each other. The shaded areas are explained in the main text.

at an even lower shaking strength [around 2.90×10^3 $(\mathrm{m/s})^{-2}$] it remains the only stable state in the system. In the rest of this paper we will fully explain the observed cascade of convection patterns using a dynamical flux model.

III. FLUX MODEL

The quantitative analysis of the observations discussed in the previous section will be based on the flux model introduced in [13]. Here we will describe the properties of this flux model in detail, followed by its application to the analysis of the two-compartment granular fountain.

A. The flux function

Clustering in compartmentalized granular gases is known to be well described by a flux model originally formulated by Eggers [6,14]. The main constituent of this model is a flux function, which gives the outflow from the k^{th} compartment (into each of its neighbors) as a function of its contents, which we here represent by n_k, being the particle fraction in compartment k with respect to the uniform distribution. (That is, $n_k=N_k/N_{\mathrm{av}}$, where N_k is the number of particles in compartment k and $N_{\mathrm{av}}=N_{\mathrm{tot}}/K$, with N_{tot} the total number of particles in the K-compartment system). As was shown in [13] for the two-compartment granular fountain, the flux function for the system at hand is given by

$$H(n_k) = F(n_k) + G(n_k) = An_k^2 e^{-Bn_k^2} + \lambda An_k^2. \tag{1}$$

Here $F(n_k)$ represents the outflux from compartment k through the slit (at height h) and $G(n_k)$ the outflux through the hole at the bottom. In [13] it was shown that such a flux model very nicely describes the experimental and numerical results for the two-compartment fountain (cf. Fig. 2). $H(n_k)$ contains two important parameters, B and λ, the significance of which will be addressed below. The third parameter A is of less relevance in the present context: It defines the absolute rate of the flux (i.e., the speed of the dynamics) and will be set to 1 by a redefinition of the time scale.

The functional form of $F(n_k)$ can be motivated from the kinetic theory of granular gases, and contains the important dimensionless driving parameter [6,7]

$$B = 4\pi \frac{gh}{(af)^2}(1-e^2)^2(r^2 N_{\mathrm{tot}}/\Omega)^2. \tag{2}$$

This consists of three dimensionless groups. The first group is proportional to the ratio between the energy a grain needs to jump from the bottom to the slit at height h and the energy it gets from collisions with the vibrating bottom plate. The second group $(1-e^2)^2$ is a measure of the dissipation in the gas, with e being the normal coefficient of restitution of the interparticle collisions. The third group is the square of a filling factor defined as the sum of cross sections of all particles $\pi r^2 N_{\mathrm{tot}}$ divided by the bottom area of a compartment Ω. For our purposes, the most important feature of B is its inverse proportionality to the driving strength $(af)^2$, which makes it directly comparable to the quantity $(af)^{-2}$ along the horizontal axes of Figs. 4 and 5.

The function $G(n_k)$ in Eq. (1), i.e., the outflux through the hole at the bottom, is obtained by simply taking the limit $h\to 0$ of $F(n_k)$, which is equivalent to setting $B=0$. One further has to account for the fact that the hole and the slit differ in size, which is done via the parameter λ, the ratio of the fluxes through hole and slit in the limit $B\to 0$ of very strong shaking.

The magnitude of the convective current can be calculated either as the net flux through the slit or through the bottom hole (the two are equal in a steady state, apart from their sign): $G(n_1)-G(n_2)=\lambda[n_1^2-(2-n_1)^2]=\lambda[-4+4n_1]=2\lambda[(n_1-n_2)]$. Here we see that [given the form of the flux function in Eq. (1)] the magnitude of the current is directly proportional to the difference between the fractions in the two compartments. Naturally, the current vanishes in the uniform state $n_1=n_2$.

Here we note that the main qualitative features of the fountain cascade are independent of the exact functional expressions for F and G, as long as they have the following general form: (1) $F(n_k)$ should go to zero in both limits $n_k=0$ and $n_k\to\infty$, and attain a maximum in between; (2) $G(n_k)$ should increase monotonically from $G(0)$; (3) the sum of F and G (i.e., H) should be a nonmonotonic function of n_k.

The functions $F(n_k)$ and $G(n_k)$ in Eq. (1) clearly meet the first two requirements. The third requirement sets a limit to

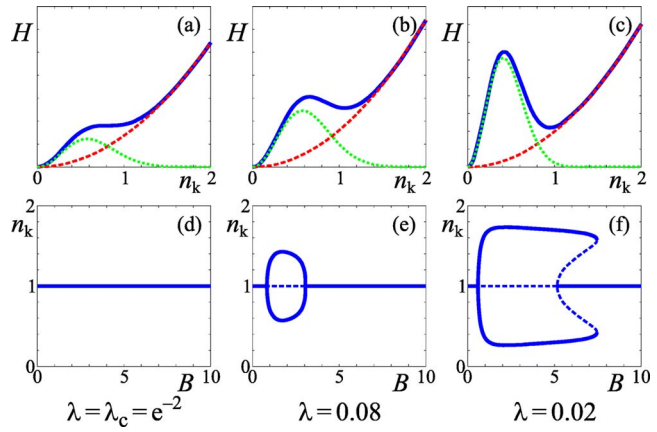

FIG. 6. (Color online) Top row: The outflux $H(n_k)$ from compartment k as a function of its particle contents n_k [(blue) solid curves], being the sum of the flux through the slit $F(n_k)$ [(green) dotted curves] and the flux through the hole $G(n_k)$ [(red) dashed curves], for three different values of the parameter λ (related to the size of the hole). (a) The critical value $\lambda_c=e^{-2}\approx 0.1353$, $B=0.75$; (b) $\lambda=0.08$, $B=0.75$; (c) $\lambda=0.02$, $B=1.50$. Bottom row: The associated bifurcation diagrams for the two-compartment system. (d) For $\lambda\geq\lambda_c$ the hole is too large to allow for clustering, so the system always remains uniform; (e) at $\lambda=0.08$ there is an interval of B values for which the uniform state is unstable (dashed) and the system goes into a stable convective clustered state; (f) for $\lambda=0.02$ we see again a new feature, namely, an interval ($5.0\lesssim B\lesssim 7.5$) where the uniform and convective state are both stable; the corresponding size of the hole is close to its minimum value of one particle diameter.

the value of λ, as follows: The first derivative of the combined flux function $H(n_k)$,

$$\frac{dH}{dn_k}=2n_k(1-Bn_k^2)e^{-Bn_k^2}+2\lambda n_k, \tag{3}$$

is a third-order polynomial, partly modified by the monotonic positive function $\exp(-Bn^2)$, so it has potentially three roots. One of these roots is $n_k=0$ [where $H(n_k)$ has a minimum] and the two other roots, if they are real, correspond to a local maximum and minimum of $H(n_k)$; see Figs. 6(b) and 6(c). The limit to the value of λ corresponds to the case when this maximum and minimum coincide (forming one inflection point with zero slope) as in Fig. 6(a); beyond this value the function $H(n_k)$ becomes monotonically increasing and does not allow for clustering any longer. The critical case is determined by $dH/dn_k=d^2H/dn_k^2=0$, or equivalently

$$\frac{dF}{dn_k}=-\frac{dG}{dn_k} \quad \text{and} \quad \frac{d^2F}{dn_k^2}=-\frac{d^2G}{dn_k^2}. \tag{4}$$

Dividing the latter two equations we find that the inflection point is located at $n_k=\sqrt{2/B}$, and inserted in Eq. (3) (with $dH/dn_k=0$) this leads to

$$\lambda_c=e^{-2}\approx 0.1353. \tag{5}$$

In Fig. 6(a) we have depicted the function $H(n_k)$ for this critical value of λ, which indeed shows an inflection point at $n_k=\sqrt{2/B}=1.63$. For $\lambda<\lambda_c$ the function $H(n_k)$ is nonmonotonic [Figs. 6(b) and 6(c)] and the outflux from two adjacent compartments with different values of n_k can now balance each other, i.e., clustering is possible.

B. Analysis of the fountain for $K=2$

The time evolution of the two-compartment granular fountain is given by a balance equation, which reflects that the time rate of change of the particle fraction in either of the two compartments is given by the inflow from its neighbor minus the outflux towards the neighbor:

$$\frac{dn_k}{dt}=H(2-n_k)-H(n_k), \tag{6}$$

where we have used the fact that the particle fractions should sum up to 2 ($=K$).

Equation (6) can be viewed as the relaxation dynamics of the variable n_k in a one-dimensional potential landscape with derivative $H(n_k)-H(2-n_k)$. Hence, in the long-time limit n_k will necessarily converge toward a steady state. The steady states of the two-compartment system are found by setting dn_k/dt to zero in Eq. (6) and assessing the linear stability of such a fixed point [7]: It is stable if $d(dn_k/dt)/dn_k<0$ at the fixed point, i.e., if the first derivative of the above balance equation (6) is negative. In that case, dn_k/dt is positive for n_k just below the fixed point, and negative for n_k just above it, so any fraction in the neighborhood of the fixed point is automatically driven toward it.

Equation (6) is identically zero for $n_k=1$, so the uniform distribution is an equilibrium for all values of B and λ. Whether it is stable depends on the sign of the first derivative

$$\left.\frac{d}{dn_k}\left(\frac{dn_k}{dt}\right)\right|_{n_k=1}=-2\left.\frac{dH}{dn_k}\right|_{n_k=1}=-4[(1-B)e^{-B}+\lambda]. \tag{7}$$

If $\lambda\geq\lambda_c$, this expression is negative for all values of B, i.e., the uniform state is stable at any shaking strength. For these large values of λ the hole at the bottom is too large to allow for any other state; some hint of clustering (as in the setup with a slit only) may occasionally take place, but the flux through the hole will soon equalize the contents of the two compartments again and thus prevent the formation of a clustered convective state. At the critical value $\lambda=\lambda_c$ there is exactly one B value for which the expression (7) is zero, namely, $B=2$.

Making the hole smaller, for $\lambda<\lambda_c$ we get an interval of B values around $B=2$ [bounded by the two solutions of $\lambda=(B-1)e^{-B}$] on which Eq. (7) is positive. Here the uniform distribution is unstable and has given way to a stable clustered, convective state. In Fig. 6(e) (for $\lambda=0.08$) we see that in first instance this clustered state exists only for those B values for which the uniform state is unstable. However, Fig. 6(f) (for $\lambda=0.02$) shows that a further reduction of the hole favors the formation of the clustered state to such a degree that the B interval for which this state exists exceeds the interval of instability of the uniform solution. In other words, there is now a B interval on which both the uniform and the convective states are stable.

The value of λ at which the convective state extends its existence beyond the unstable region of the uniform state [i.e., where the associated pitchfork bifurcation turns from a sub- into a supercritical one; see Figs. 6(e) and 6(f)] can be found by performing a Taylor expansion of the stability criterion [Eq. (7)] around the uniform distribution. Setting $n_k=1+\epsilon$ we find

$$\frac{d(d\epsilon/dt)}{d\epsilon} = -H'(1-\epsilon) - H'(1+\epsilon) = -4[(1-B)e^{-B}+\lambda] + 4Be^{-B}(2B^2-9B+6)\epsilon^2 + O(\epsilon^4), \quad (8)$$

where H' denotes the derivative of H to n_k, or equivalently to ϵ [cf. Eq. (3)]. In the two bifurcation points at $n_k=1$ ($\epsilon=0$), where the convective state merges with the uniform state, the constant term in the above expansion is equal to zero. The transition from a sub- to supercritical bifurcation occurs when also the quadratic term in the Taylor expansion Eq. (8) vanishes: at that moment the second pitchfork bifurcation in Fig. 6(e) changes its leftward curve into a rightward curve, going momentarily (and locally, where it branches off the horizontal line $n_k=1$) through a vertical position. So the transition takes place when $B_{\mathrm{tr}}=(9+\sqrt{33})/4\approx 3.6861$, leading to $\lambda_{\mathrm{tr}}=(B_{\mathrm{tr}}-1)\exp(-B_{\mathrm{tr}}) \approx 0.067\,338$.

Finally, if the hole becomes smaller than the particle diameter, no flux through the hole is possible any longer and we should recover the bifurcation diagram of the system with a slit only [7,8]. There is no critical value of λ associated with this in our flux model, since the model bypasses the particle nature of the granular material (the fractions n_k can vary continuously), yet in the limit for $\lambda\to 0$ one indeed sees that the left-hand pitchfork bifurcation goes to $B=1$ and the right-hand pitchfork bifurcation is shifted toward $B\to\infty$ (meaning that the uniform distribution remains unstable even for extremely weak shaking). Consequently, also the stability region of the clustered convective state is stretched up to $B\to\infty$. These are precisely the characteristics of the bifurcation diagram for the system with a slit only [6–8].

The theoretical prediction from the flux model compares well to the results from experiments and simulations for the two-compartment system [13]. For our experimental setup one finds as a rough estimate $\lambda\approx 0.02$ under the assumption that the finite particle radius effectively reduces the dimensions of slit and hole by 1.8 mm and neglecting any velocity anisotropies. When fitted with $\lambda=0.018$, the comparison of flux model and experiment in Fig. 2 is good; especially the bifurcation and the hysteresis are well reproduced.

IV. ANALYSIS FOR K COMPARTMENTS

In this section we present the technique to construct bifurcation diagrams for arbitrary number of compartments K. We explicitly work out the cases $K=3$ and $K=5$ finding good agreement with the numerical diagrams found earlier. We conclude with some general remarks on the structure of the cascade of convective states for arbitrary K.

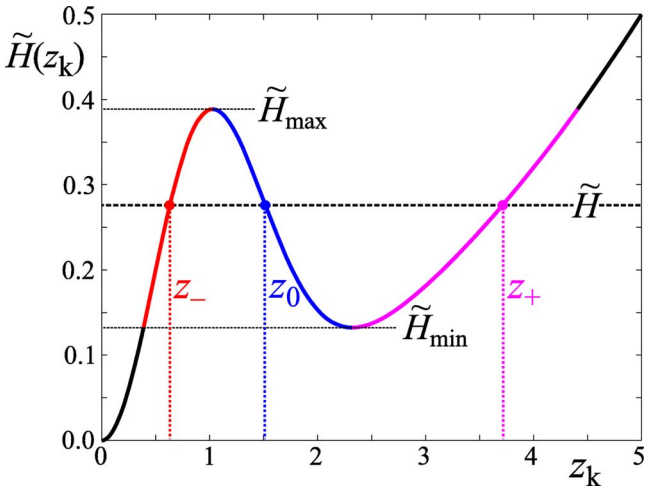

FIG. 7. (Color online) Flux function $\tilde{H}(z_k)$ as a function of the new variable $z_k=\sqrt{B}n_k$, for a fountain setup with a relatively small hole ($\lambda=0.02$). The steady states of the system must satisfy the constant-flux condition represented by the dashed horizontal line [Eq. (13)]. For $\tilde{H}_{\min}<\tilde{H}<\tilde{H}_{\max}$ this condition has three solutions z_-, z_0, and z_+ (which may be combined in any order to construct a steady state; see Fig. 8), whereas for $\tilde{H}$ outside this interval there is only one solution, which means that in these regimes only a uniform steady state exists.

A. Matrix formulation of the problem

Given the flux function [Eq. (1)] we can directly write down the balance equation for a system consisting of arbitrarily many compartments:

$$\frac{dn_k}{dt} = H(n_{k-1}) - 2H(n_k) + H(n_{k+1}), \quad (9)$$

for $k=1,\ldots,K$. For simplicity, we will use cyclic boundary conditions $n_{K+1}=n_1$ (otherwise the end boxes should be treated separately). The above balance equation is supplemented by the condition $\Sigma n_k=K$, related to the conservation of the total number of particles N_{tot}. Equation (9) for all K compartments together can conveniently be written in matrix form:

$$\frac{d\mathbf{n}}{dt} = \mathbf{M}\cdot\mathbf{h} \quad \text{or} \quad \frac{dn_k}{dt} = \sum_{l=1}^{K} M_{kl}H(n_l), \quad (10)$$

where $\mathbf{n}$ is a K-dimensional vector containing the fractions n_k, $\mathbf{h}$ is a vector with components $H(n_k)$, and $\mathbf{M}$ is a so-called tri-diagonal $K\times K$ matrix with elements -2 on the diagonal and 1 on all first off-diagonal positions, as well as on the corners $(1,K)$ and $(K,1)$. This matrix has the following important properties [8]: its rank is $K-1$ and its kernel (corresponding to the eigenvalue zero) is the linear subspace spanned by the eigenvector $\mathbf{1}=(1,1,\ldots,1)$. It is also negative semidefinite, meaning that $\mathbf{h}\cdot\mathbf{M}\cdot\mathbf{h}<0$ unless $\mathbf{M}\cdot\mathbf{h}=0$. As a consequence all other eigenvalues of $\mathbf{M}$ are negative.

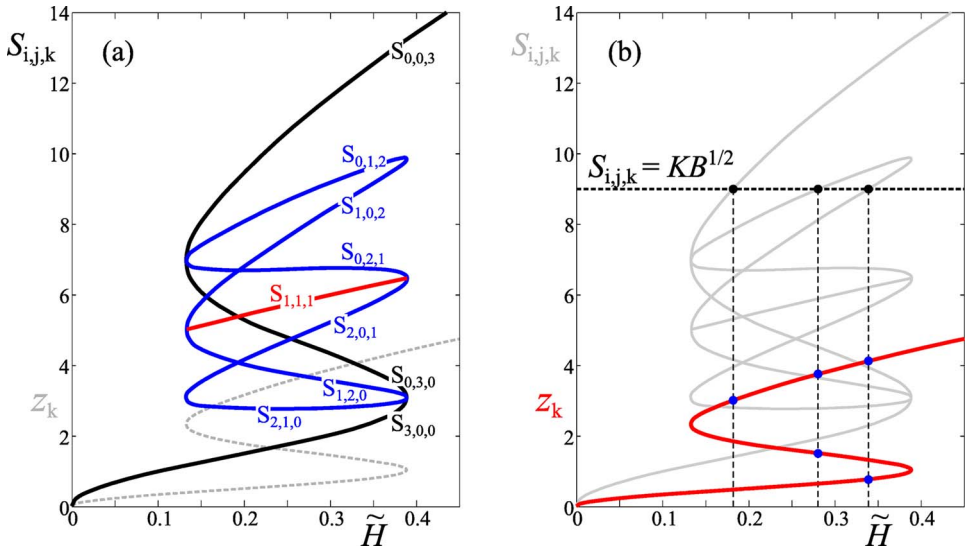

FIG. 8. (Color online) (a) The ten sum functions $S_{i,j,k}$ for $K=3$ compartments, i.e., the sum of i times z_- (on the lower branch of the dashed gray S-shaped curve), j times z_0 (on the middle branch), and k times z_+ (on the upper branch), with $i+j+k=K=3$. The uniform state (with three equal components) is represented by the successive sum functions $S_{3,0,0}$, $S_{0,3,0}$, and $S_{0,0,3}$ (solid black lines); each transition from one sum function to the next signals a bifurcation and associated change of stability. The one-cluster state is represented by the sum functions $S_{2,1,0}$, $S_{2,0,1}$, and $S_{0,2,1}$, respectively. The two-cluster state is represented by $S_{1,2,0}$, $S_{1,0,2}$, and $S_{0,1,2}$. Finally, the central sum function $S_{1,1,1}$ (solid red line) corresponds to a state with a different fraction in each of the three compartments. (b) Graphical representation of the conservation condition $S_{i,j,k}(\tilde{H})=K\sqrt{B}$ [Eq. (15)], from which (given any value of B, here $B=9$) the steady-state fractions z_k are determined. These are the solid dots (blue) on the S-shaped curve (red), which—translated back to the fractions $n_k=z_k/\sqrt{B}$—yield the bifurcation diagram of Fig. 9.

To find the fixed points of Eq. (10) we have to solve $\mathbf{M}\cdot\mathbf{h}=0$, from which we can immediately conclude that $\mathbf{h}$ should be in the kernel of $\mathbf{M}$, i.e., proportional to $\mathbf{1}$. This means that all the elements of the flux vector $\mathbf{h}$ should be equal:

$$H(n_k) = \text{const} \quad \text{for all } k = 1, \ldots, K. \tag{11}$$

From Figs. 6(a)–6(c) it is clear that for $\lambda \geq \lambda_c$ this constant-flux condition is only satisfied by the uniform state in which all compartments are equally filled, but for $\lambda < \lambda_c$ there exist clustered solutions to Eq. (11) with two or even three different densities (distributed arbitrarily over the K compartments), all corresponding to the same value for the flux.

Since Eq. (10) represents a nonlinear evolution equation in several dimensions (in fact $K-1$ dimensions), in general not only steady states (fixed points), but also periodic or even chaotic solutions may be possible in the long-time limit. The latter two possibilities are ruled out in the Appendix with the help of a Lyapunov function. Hence, in order to discuss the long-time asymptotics of Eq. (10) we can focus on steady states.

B. Constructing the bifurcation diagram

To construct the bifurcation diagram (i.e., the fixed points as a function of the driving parameter B) for arbitrary K, we use the method that we developed in [8].

First we note that the B dependence of the flux function $H(n_k)$ [Eq. (1)] can be transferred to the conservation condition $\Sigma n_k = K$ by a simple change of variables:

$$z_k \equiv \sqrt{B} n_k, \tag{12}$$

which (up to an irrelevant multiplicative constant A/B) transforms $H(n_k)$ into $\tilde{H}(z_k) = z_k^2 \exp(-z_k^2) + \lambda z_k^2$ (independent of B) and $\Sigma n_k = K$ into $\Sigma z_k = K\sqrt{B}$. The fixed points of Eq. (10) can now be found by solving

$$\tilde{H}(z_k) = \text{const}, \quad \sum_{k=1}^{K} z_k = K\sqrt{B}. \tag{13}$$

In words, we have to find all possible sets of fractions z_k (equal or not, but corresponding to the same flux) that add up to $K\sqrt{B}$. The procedure is illustrated in Figs. 7–9.

Below $\tilde{H}_{\min}$ and above $\tilde{H}_{\max}$ (see Fig. 7) there is just one solution to $\tilde{H}(z_k)=\text{const}$, which together with $\Sigma z_k = K\sqrt{B}$ means that all z_k must be equal to $\sqrt{B}$. This is the uniform distribution $n_k=1$ $(k=1,\ldots,K)$. In contrast, between $\tilde{H}_{\min}$ and $\tilde{H}_{\max}$ there are *three* solutions to $\tilde{H}(z_k)=\text{const}$, namely, z_-, z_0, and z_+, and all possible distributions (over the K compartments) of these three solutions with $\Sigma z_k = K\sqrt{B}$ are steady states.

To systematically find all those states we construct the sum functions $S_{i,j,k}(\tilde{H})$, which represent the distributions containing i times z_-, j times z_0, and k times z_+,

$$S_{i,j,k}(\tilde{H}) = i z_-(\tilde{H}) + j z_0(\tilde{H}) + k z_+(\tilde{H}), \tag{14}$$

for all combinations of i,j,k ranging from 0 to K with $i+j+k=K$. For example, for $K=3$ there are ten sum functions, all of which are depicted in Fig. 8(a). Given these

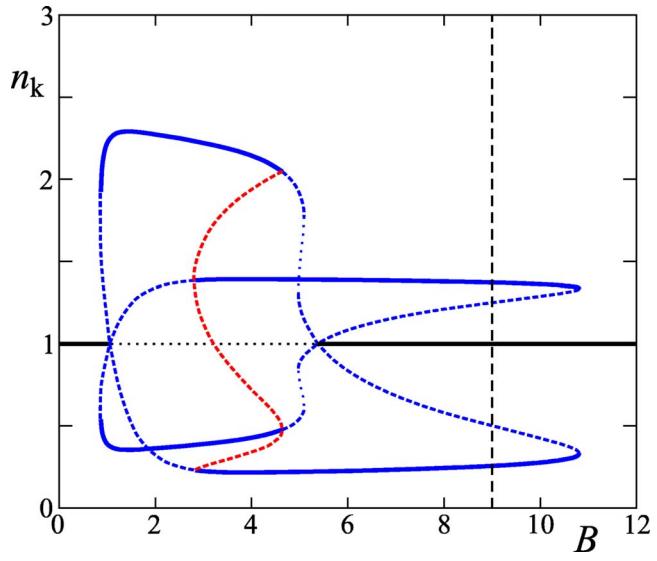

FIG. 9. (Color online) Bifurcation diagram of the three-compartment system, evaluated from the flux model. It shows both the stable steady states (solid lines), which agree well with the ones found from numerical experiments in Fig. 4, and the unstable states (dashed lines). The S-shaped curve at $B \approx 4$ (red) corresponds to a steady state that is always unstable, consisting of three different fractions n_k in the three compartments. The dashed line at $B=9$ is the counterpart of the horizontal dashed line in Fig. 8(b); the three coexisting steady states at this value of B (uniform state, unstable two-cluster state, and stable two-cluster state) are discussed in the text.

functions, the steady states are now determined (for any value of B) by solving

$$S_{i,j,k}(\tilde{H}) = K\sqrt{B}. \tag{15}$$

This is graphically illustrated in Fig. 8(b), where the steady states for $B=9$ are given by the intersection points of the sum functions $S_{i,j,k}$ with the horizontal line $K\sqrt{B}=9$.

For this value of B, there are three intersection points. The leftmost of these lies on the sum-function $S_{0,0,3}$, so this is the uniform distribution $\{z_+, z_+, z_+\}$; the middle intersection point lies on $S_{0,1,2}$, corresponding to a steady two-cluster state that consists of one compartment with a fraction z_0 and two with a fraction z_+ (i.e., any of the three cyclic permutations of $\{z_0, z_+, z_+\}$); and the rightmost intersection point (also a two-cluster state) lies on $S_{1,0,2}$, corresponding to any of the three permutations of $\{z_-, z_+, z_+\}$).

This information is then translated back to the original fractions $n_k = z_k/\sqrt{B}$ and plotted in the bifurcation diagram of Fig. 9. Indeed, at the value $B=9$ we see the three steady states found above: (1) The uniform state $\{n_1, n_2, n_3\} = \{1,1,1\}$ on the solid (black) line, (2) the threefold-degenerate state $\{n_1, n_2, n_3\} \approx \{0.50, 1.25, 1.25\}$ on the dashed (blue) curves, and (3) the threefold-degenerate state $\{n_1, n_2, n_3\} \approx \{0.24, 1.38, 1.38\}$ on the solid (blue) curves. As before, the solid lines stand for stable states, whereas the dashed lines represent unstable ones.

The stability of the states is determined by means of a linear stability analysis, i.e., from the eigenvalues of the Jacobi matrix **J** associated with Eq. (10). The components of this matrix are

$$J_{jk} = \frac{\partial \dot{n}_j}{\partial n_k} = \sum_l M_{jl} H'(n_l) \frac{\partial n_l}{\partial n_k} = M_{jk} H'(n_k), \tag{16}$$

where H' denotes the derivative of H with respect to n [given explicitly in Eq. (3)]. The method is analogous to the stability analysis that has been described in [8].

C. Bifurcation diagram characteristics

It is interesting to compare the theoretical bifurcation diagram from the flux model (Fig. 9, for $\lambda = 0.02$) with the diagram obtained via numerical experiments (Fig. 4). We see that the stable branches agree very well, even in the subtle discontinuous character of the first transition (at small B) where the hot uniform state gives way to the one-cluster fountain state.

There is only one small quantitative difference, namely, in the filling fractions: in experiment the cluster fractions are about 10% higher than the theoretical prediction. This may be traced back to the flux function $G(n_k)$ in Eq. (1), which for growing cluster fractions n_k overestimates the flux through the hole: When n_k becomes very large, the flux through the hole in reality does not grow without bound but saturates on a constant level, so big clusters are drained less than the current flux model predicts. This may be mended by including a saturation factor $G(n_k) = \lambda A n_k^2 (1 + \beta n_k^2)^{-1}$, which—at the cost of introducing a fit parameter β into the model—indeed yields somewhat larger clusters. By tuning the value of β the cluster sizes can be made to coincide with the numerically observed ones.

The unstable branches in the bifurcation diagram of Fig. 9, which are of course not found in the numerical experiments, show the intricate underlying structure that connects the stable steady states. One branch deserves particular attention, since the state corresponding to it never becomes stable, but only serves to properly stabilize and destabilize the one- and two-cluster states: this is the S-shaped branch (dashed red curve) at $B \approx 4$. It corresponds to a state in which the three compartments all contain a different particle fraction, positioned on the three different parts of the S-shaped curve. This state varies continuously from a two-cluster state at $B=2.8$ to a one-cluster state at $B=4.6$. The same continuous crossover can also be inferred from Fig. 8(a), where the associated sum function $S_{1,1,1,}$ (solid red curve) is seen to connect the two-cluster function $S_{1,2,0}$ (at the point where it goes over into $S_{1,0,2}$) with the one-cluster function $S_{2,0,1}$ (at the point where it goes over into $S_{0,2,1}$).

It is worthwhile to have a closer look at the bifurcational structure of the three-compartment system, and this is done in Fig. 10 at six successive points for increasing values of B. The six triangular plots represent the configuration space spanned by the fractions n_1, n_2, and n_3. The lower left corner of each plot corresponds to the state $\{n_1, n_2, n_3\} = \{3,0,0\}$ (all material in compartment 1), the lower right corner to $\{0,3,0\}$, and the upper corner to $\{0,0,3\}$ [15]. The center of the triangle corresponds to the uniform

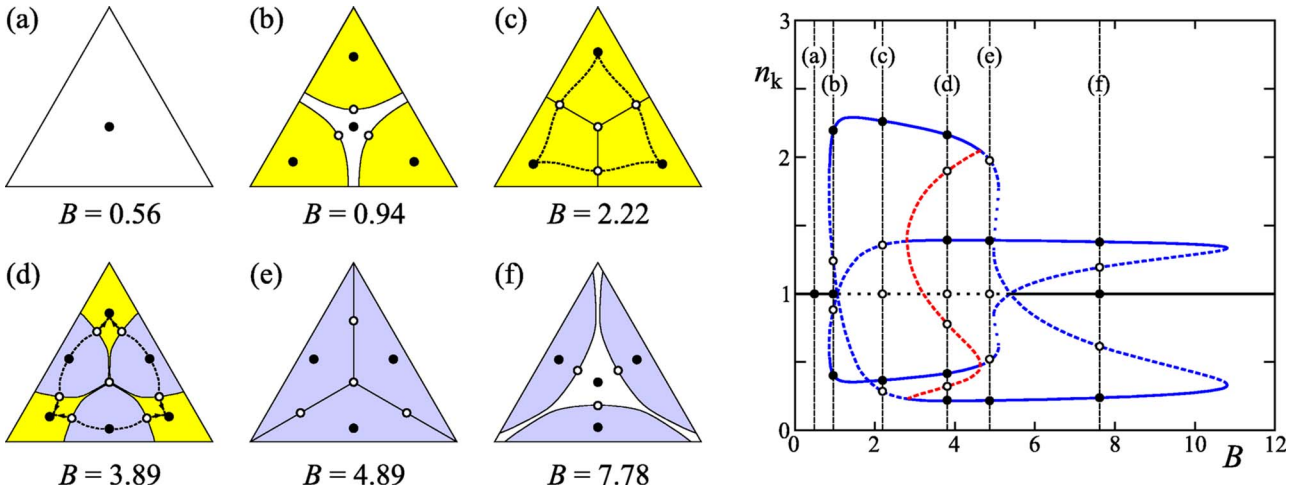

FIG. 10. (Color online) Bifurcation structure of the three-compartment granular fountain, highlighted at six successive values of the parameter B. The triangular plots (a)–(f) depict the configuration space, as explained in the text; white regions indicate the basin of attraction of the uniform steady state (the fixed point in the center), light gray (yellow) regions correspond to the three one-cluster states (the fixed points toward the corners of the triangle), and dark gray (blue) regions correspond to the three two-cluster states (the fixed points close to the middle of the sides of the triangle). Beyond $B \approx 11$ the situation of plot (a) is recovered again.

state $\{1,1,1\}$, which is present (in the form of a dot) in each of the six plots. Solid dots denote stable steady states, and open dots denote unstable ones. The different shadings represent the basins of attraction of the various steady states: white corresponds to the uniform state, light gray (yellow) to a one-cluster state, and dark gray (blue) to a two-cluster state.

In Fig. 10(a), for $B=0.56$ (strong shaking), only the uniform fixed point in the center exists. Being the only steady state, it is naturally stable. Any initial configuration (every point within the triangle) evolves toward it.

In Fig. 10(b), at $B=0.94$, the stable one-cluster state has just come into existence. It is threefold degenerate (since the cluster can be located in any of the three compartments) and is represented by the three solid dots toward the corners of the triangles. It has been created together (via a saddle-node bifurcation, at a B value slightly smaller than the present one) with an unstable one-cluster state. This twin state (represented by the open dots, also threefold degenerate) lies exactly on the boundary between the basins of attraction of the one-cluster state [light gray (yellow)] and the uniform state (white). It closes in upon the uniform state as B grows, diminishing its basin of attraction, and goes right through it at a value just beyond $B=1$. At that moment the white basin of attraction vanishes and the uniform fixed point becomes unstable.

Figure 10(c), at $B=2.22$, shows that the unstable one-cluster state has passed through the central fixed point and is now positioned at the other side of the uniform state. This means that the compartment that previously had a fraction n_k exceeding 1 now contains *less* than 1; vice versa, the two compartments that had fractions less than 1 now contain *more* than 1. So after its passage through the uniform state the unstable one-cluster state has become an unstable two-cluster state. This is also apparent from the bifurcation diagram: The dashed (blue) lines that cross the uniform state (just beyond $B=1$) represent a one-cluster state to the left of this intersection point, but a two-cluster state to the right of it.

The whole triangle is now light gray (yellow), i.e., every initial condition leads to one of the three one-cluster states. The dashed lines that have been drawn in the configuration space depict the stable and unstable manifolds (eigenvectors) of the various fixed points. The eigenvectors of the fixed point in the center are directed toward the unstable two-cluster states. These two-cluster states have two stable directions and two unstable ones (i.e., they are saddle points), with the unstable ones being directed toward the stable one-cluster states. Thus, if one starts out from an initial state close to the uniform distribution, the dynamics is such that the system first passes close by the unstable two-cluster state before it eventually arrives at the one-cluster state. The two-cluster state is a so-called transient.

The next stage is depicted in Fig. 10(d), at $B=3.89$. The one-cluster state is still stable, and also the unstable two-cluster has gained stability through a pitchfork bifurcation in which *two* unstable fixed points are created per two-cluster. These are the six open dots that lie on the boundaries between the basins of attraction of the two-cluster states [dark gray (blue)] and those of the one-cluster states [light gray (yellow)]. They represent the crossover state we encountered before (associated with the sum function $S_{1,1,1}$), with a different fraction in each of the three compartments, which is obviously sixfold degenerate.

For increasing B the six unstable points move from the two- toward the one-cluster states and in Fig. 10(e), at $B=4.89$, they have just arrived there. Upon their arrival they have (in a reverse pitchfork bifurcation) made the one-cluster state unstable. So now the only stable fixed points in the diagram are the two-cluster states, and indeed the whole triangle is dark gray (blue), i.e., every initial state leads to a two-cluster state. The straight lines from the corners of the triangle toward the center (which encompass both the unstable uniform state and the three unstable one-clusters) are

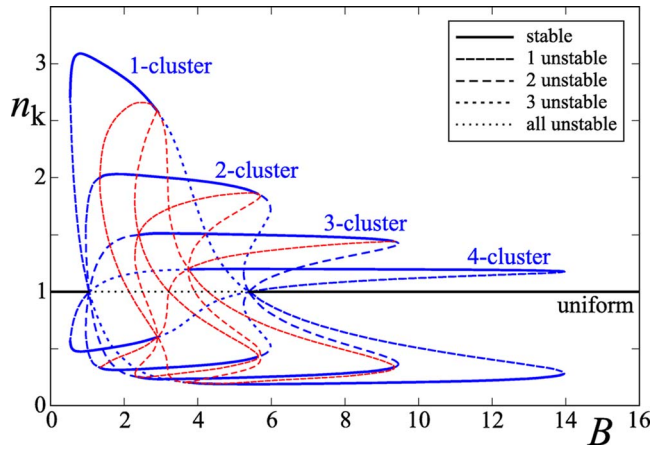

FIG. 11. (Color online) Bifurcation diagram of the five-compartment system, evaluated from the flux model with $\lambda=0.02$. The stable steady states (solid lines) agree well with the ones found from numerical experiments (Fig. 5) and are seen to be interconnected via a whole maze of unstable steady states (dashed lines, increasingly fragmented with increasing number of unstable eigenvalues). Among the unstable states are also six states with three different particle fractions [the S-shaped (red) lines]; these never become stable, but play an important role in stabilizing and destabilizing the regular fountain states with only two different fractions.

the boundaries between the regions of attraction of the three permutations of the two-cluster state.

In Fig. 10(f), at $B=7.78$, the three unstable one-cluster points have traveled along these lines toward—and through—the uniform fixed point in the center. In the process, the uniform state has become stable again and the one-cluster states have turned into two-cluster states [as before; see the discussion of Fig. 10(c)]. This is also seen in the bifurcation diagram.

The basins of attraction at this value of B show an interesting feature: If one starts out with all beads in one single compartment (say $\{3,0,0\}$ in the lower left corner of the plot), the system will eventually end up in the uniform state, since the corners of the triangle lie in the white basin of attraction. This may, however, take quite some time since the system has to pass through a narrow channel in the configuration space. In an experimental situation, i.e., in the presence of statistical fluctuations, the system may even be kicked out of the channel and into the dark gray (blue) basin of attraction—ending up in a two-cluster state. In our numerical experiments on the three-compartment system we have always been able to avoid this effect, but for five compartments (when the channels are even narrower, and the configuration space more intricate as a whole) we have encountered it in the form of the shaded data sets in Fig. 5. All these data originated from a state with all beads in one compartment, which either got stuck there or (by a statistical fluctuation) were kicked into the basin of attraction of a three-cluster state.

After stage Fig. 10(f), around $B=11$, the unstable two-cluster states and their stable counterparts meet and annihilate each other (in a reverse saddle-node bifurcation), leaving only the stable fixed point in the middle of the triangle. The resulting configuration space is just the same as the one depicted in Fig. 10(a): every initial condition leads to the uniform state again.

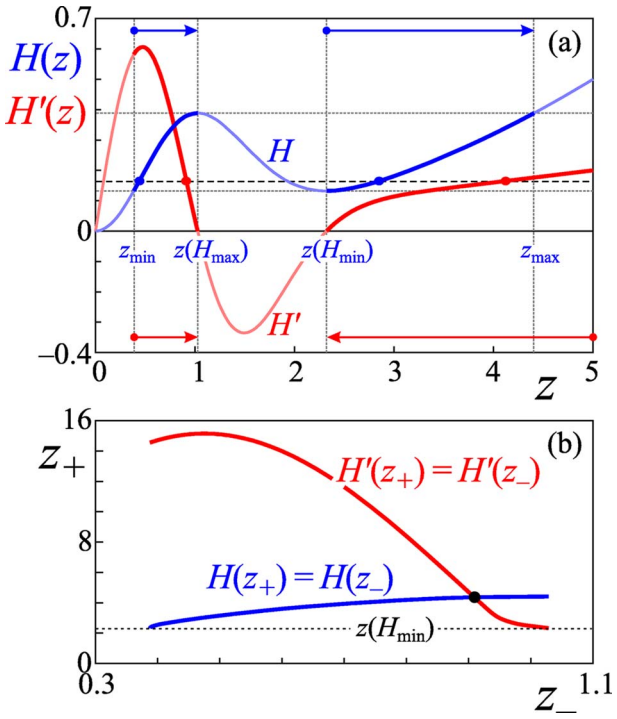

FIG. 12. (Color online) Construction of a stable two-fraction fountain state, with the hot (dilute) compartments containing a fraction $z_-/\sqrt{B}$ and the cold (dense) compartments $z_+/\sqrt{B}$. (a) The flux function $H(z)$ (blue curve) and its derivative $H'(z)$ (red curve) for $\lambda=0.02$. The solid dots are pairs of points that satisfy the flux balance $H(z_+)=H(z_-)$ and the derivative equality $H'(z_+)=H'(z_-)$, respectively. The arrows indicate the direction in which these pairs evolve as the shaking parameter B is increased. (b) The curves of z_+ vs z_- corresponding to the condition $H(z_+)=H(z_-)$ (blue) and to $H'(z_+)=H'(z_-)$ (red). These curves cross each other in one point: the corresponding two-fraction state is stable, as explained in the text.

D. Beyond $K=3$ compartments

The analysis for $K=3$ compartments can be extended analogously to any number of compartments. As an example in Fig. 11 we give the bifurcation diagram for $K=5$ compartments, also for $\lambda=0.02$, which may be compared to the numerically obtained diagram in Fig. 5. Again the stable branches agree reasonably well, and the flux model reveals how they are connected to each other by a complex maze of unstable branches. The three-fraction states (that never become stable) have become more frequent than in the case $K=3$, and they are seen to play an important role in stabilizing and destabilizing the regular fountain states, which have only two different fractions. The diluted branches are better distinguishable than in the molecular dynamics situations, which can be attributed to the presence of noise in the latter. Moreover, in the simulations the clustering is somewhatmore pronounced, and hence the depleted compartments are more dilute. The largest difference is found for the one-cluster state where for increasing B the model predicts a *decrease* of

the cluster size, whereas the simulations show a slight increase (cf. Fig. 5). Including a saturation factor as explained in the previous subsection can only partly repair this difference. However, the dynamics in the highly clustered region is very slow, so it may well be that in the simulation the system was still on its way to the true stable one-cluster state (or even got stuck) and that therefore the cluster size in Fig. 5 was overestimated.

The number of branches in the bifurcation diagram is directly related to the number of sum functions $S_{i,j,k}$, which for general K is equal to $\frac{1}{2}(K+1)(K+2)$, as can be shown by enumerating all possible combinations of i, j, and k under the condition $i+j+k=K$. Three of these functions correspond to the uniform state (namely, $S_{K,0,0}$, $S_{0,K,0}$, and $S_{0,0,K}$, with only one of the three elements i,j,k being nonzero); then there are $3K-3$ sum functions corresponding to two-fraction states (with two elements from i,j,k being nonzero); and the rest of the sum functions $[\frac{1}{2}(K+1)(K+2)-3K=\frac{1}{2}(K-1)(K-2)$ of them] correspond to three-fraction states for which all three elements i,j,k are nonzero. These are in general unstable.

For any $K\geq 2$ it can be proven that each of the successive two-fraction fountain states has an associated interval of B values on which it is stable. This is illustrated in Fig. 12, where we explicitly construct such a stable two-fraction state.

In Fig. 12(a) we have depicted the flux function $H(z)$ (for $\lambda=0.02$, but any λ smaller than λ_c would do), and we concentrate on the situation which consists of z_- and z_+, i.e., the two fractions corresponding to the left and right branches of $H(z)$ (cf. Fig. 7). This situation comes into existence (at a certain value of B) with the two fractions $\{z_-,z_+\}=\{z_{\min},z(H_{\min})\}$. For increasing B the fractions gradually evolve toward $\{z_-,z_+\}=\{z(H_{\max}),z_{\max}\}$, always such that $H(z_-)=H(z_+)$, ensuring the flux balance throughout the K-compartment array. This evolution for growing B is indicated by the top (blue) arrows in the upper part of Fig. 12(a).

In the same figure we have plotted the derivative of the flux function $H'(z)$, and we follow the two fractions z_-^* and z_+^* that satisfy the condition $H'(z_-)=H'(z_+)$. As B increases, these two fractions evolve from $\{z_-^*,z_+^*\}\approx\{z_{\min},15.3\}$ toward $\{z_-^*,z_+^*\}=\{z(H_{\max}),z(H_{\min})\}$. The evolution of the pair $\{z_-^*,z_+^*\}$ for growing B is indicated by the (top) red arrows in the lower part of Fig. 12(a).

In Fig. 12(b) we plot two curves: (a) The first one shows z_+ vs z_- corresponding to the flux balance $H(z_+)=H(z_-)$ (blue curve). In agreement with the blue arrows in Fig. 12(a) (which both point in the positive direction) this is a monotonically increasing function of z_-, from $z(H_{\min})$ to some higher value. (b) Second, we plot z_+^* vs z_-^* corresponding to the second condition $H'(z_+)=H'(z_-)$ (red curve). This is a decreasing function of z_- [in agreement with the direction of the red arrows in Fig. 12(a)], starting from some high value and ending at $z(H_{\min})$. Since the first curve starts from $z(H_{\min})$ and the second one ends at this same value, the two functions necessarily cross each other. This yields a unique solution for which both $H(z_+)=H(z_-)$ and $H'(z_+)=H'(z_-)$ are satisfied.

For this two-fraction state the Jacobi matrix [Eq. (16)] takes the form

$$\mathbf{J}=\mathbf{M}\begin{pmatrix} H'(z_-) & \cdots & 0 & 0 & \cdots & 0 \\ \vdots & \ddots & \vdots & \vdots & & \vdots \\ 0 & \cdots & H'(z_-) & 0 & \cdots & 0 \\ 0 & \cdots & 0 & H'(z_+) & \cdots & 0 \\ \vdots & & \vdots & \vdots & \ddots & \vdots \\ 0 & \cdots & 0 & 0 & \cdots & H'(z_+) \end{pmatrix}=H'(z_+)\mathbf{M}, \tag{17}$$

or equivalently $\mathbf{J}=H'(z_-)\mathbf{M}$ at this particular point. Since $H'(z_+)$ is positive [see Fig. 12(a)] and the matrix $\mathbf{M}$ is negative definite (where we disqualify the zero-eigenvalue vector $\{\mathbf{1},\ldots,\mathbf{1}\}$, which corresponds to adding an equal amount of material to every compartment, violating the mass conservation in the system [8]), Eq. (17) implies that all eigenvalues of $\mathbf{J}$ are negative. Hence the constructed two-fraction state [with fractions z_- and z_+ given by the crossing point in Fig. 12(b)] is *stable*. And typically, if it is stable at one particular value of B, it will also be stable in some interval of B values around it.

Along the same lines we can explain the observed cascade of two-fraction fountain states in the bifurcation diagram, with the states that have more "cold" (dense) compartments occurring toward larger values of B. Indeed, when the constructed state contains many z_+ (cold compartments), then the associated B value is high, because $\sqrt{B}=(iz_-+kz_+)/K$, with $i+k=K$ [cf. Eq. (14))]. Hence the unique solution we have constructed in Fig. 12 lies toward larger B with increasing number of cold z_+ compartments: with every extra z_+, the square root of the associated B value increases with $(z_+-z_-)/K$. This shows that the cascade observed for $K=3$ and 5 exists for any number of compartments $K\geq 3$.

The above analysis can be carried out analogously for the three-fraction states. These are found to be typically unstable, because one of the three fractions corresponds to the middle branch of $H(z)$, namely, z_0, for which the derivative $H'(z_0)$ is negative. This generally leads to one or more positive eigenvalues of $\mathbf{J}$.

V. CONCLUSION

In conclusion, on the basis of our flux model we have constructed the bifurcation diagram of the granular fountain with K compartments, for any $K \geq 2$. For decreasing shaking strength [or equivalently, for increasing B, Eq. (2)] we find a stepwise transition from the uniform state with K hot compartments, to a one-cluster state (one cold compartment and $K-1$ hot ones), to a two-cluster state (two cold compartments and $K-2$ hot ones), and so on, until at some low shaking strength one arrives at the situation with K cold compartments, which is again a uniform state. For $K \geq 3$ the successive steps in this cascade are all hysteretic, first-order transitions.

The theoretical bifurcation diagram obtained from the flux model proves to be in good quantitative agreement with our molecular dynamics simulations on fountain setups with $K=3$ and 5 compartments.

ACKNOWLEDGMENTS

Special thanks are due to Detlef Lohse for the many useful discussions we had together and for reading the manuscript. This work is part of the research program of the Stichting FOM, which is financially supported by NWO. D.v.d.M. acknowledges partial support from the National Science Foundation under Grant No. PHY99-07949. P.R. was supported by the Deutsche Forschungsgemeinschaft under SFB 613, Grant No. RE 1344/3, and by the ESF program STOCHDYN.

APPENDIX: LYAPUNOV FUNCTION

In general, not only steady states (fixed points), but also periodic or even chaotic states may be possible solutions of Eq. (10) in the long-time limit. In this appendix, we rule out the existence of periodic solutions to Eq. (10) by explicitly constructing a strict Lyapunov function for the K-compartment system [16].

To this end, we first define the functions

$$\Gamma(n) := -\int_{\nu=0}^{n} H(\nu)d\nu, \tag{A1}$$

$$L(\mathbf{n}) := \sum_{k=1}^{K} \Gamma(n_k). \tag{A2}$$

With Eq. (1) it follows that $L(\mathbf{n}) \leq 0$ for any vector $\mathbf{n}$ with $n_k \in [0,1]$.

Next we compute the time derivative of L along a solution $\mathbf{n}(t)$ of the dynamics Eq. (10):

$$\begin{aligned}\frac{d}{dt}L(\mathbf{n}(t)) &= \sum_{k=1}^{K}\left(\frac{d\Gamma}{dn}\right)_{n=n_k(t)}\frac{dn_k(t)}{dt} \\ &= -\sum_{k=1}^{K}\sum_{l=1}^{K} H(n_k(t))M_{kl}H(n_l(t)) = -\mathbf{h}\cdot\mathbf{M}\cdot\mathbf{h}.\end{aligned} \tag{A3}$$

Due to the properties of $\mathbf{M}$ mentioned in Sec. IV A it follows that $dL(\mathbf{n}(t))/dt > 0$, except if $\mathbf{M}\cdot\mathbf{h}=0$ or, equivalently, if $d\mathbf{n}(t)/dt=0$. In other words, $L(\mathbf{n})$ is a so-called Lyapunov function, implying that $d\mathbf{n}(t)/dt \to 0$ for $t \to \infty$, i.e., the only possibility for $\mathbf{n}(t)$ for asymptotically long time t is to converge toward a fixed point.

[1] H. Jaeger, S. Nagel, and R. Behringer, Rev. Mod. Phys. **68**, 1259 (1996).
[2] I. Goldhirsch, Annu. Rev. Fluid Mech. **35**, 267 (2003).
[3] I. Goldhirsch and G. Zanetti, Phys. Rev. Lett. **70**, 1619 (1993).
[4] Y. Du, H. Li, and L. P. Kadanoff, Phys. Rev. Lett. **74**, 1268 (1995); see also L. P. Kadanoff, Rev. Mod. Phys. **71**, 435 (1999).
[5] A. Kudrolli, M. Wolpert, and J. P. Gollub, Phys. Rev. Lett. **78**, 1383 (1997).
[6] J. Eggers, Phys. Rev. Lett. **83**, 5322 (1999).
[7] K. van der Weele, D. van der Meer, M. Versluis, and D. Lohse, Europhys. Lett. **53**, 328 (2001).
[8] D. van der Meer, K. van der Weele, and D. Lohse, Phys. Rev. E **63**, 061304 (2001).
[9] An alternative way of supplying the required energy is by blowing air through the granular bed, e.g., via a porous bottom.
[10] R. Ramirez, D. Risso, and P. Cordero, Phys. Rev. Lett. **85**, 1230 (2000).
[11] R. D. Wildman, J. M. Huntley, and D. J. Parker, Phys. Rev. Lett. **86**, 3304 (2001).
[12] X. He, B. Meerson, and G. Doolen, Phys. Rev. E **65**, 030301(R) (2002).
[13] D. van der Meer, P. Reimann, K. van der Weele, and D. Lohse, Phys. Rev. Lett. **92**, 184301 (2004).
[14] K. van der Weele, R. Mikkelsen, D. van der Meer, and D. Lohse, in *The Physics of Granular Media*, edited by H. Hinrichsen and D. E. Wolf (Wiley-VCH Verlag, Weinheim, 2004), pp. 117–139.
[15] This configuration space is the triangle one gets by intersecting the plane $n_1+n_2+n_3=3$ with the 1/8 part of (n_1,n_2,n_3) space corresponding to non-negative n_k. One can show that the fractions n_k corresponding to an arbitrary point in this configuration space can be found by evaluating the distances from the point to the three sides of the triangle.
[16] D. K. Arrowsmith and C. M. Place, *Dynamical Systems: Differential Equations, Maps and Chaotic Behaviour* (Chapman & Hall, London, 1992).